BODY FORCES AND PRESSURES IN ELASTIC MODELS OF THE MYOCARDIUM

WILLIAM H. PIERCE, *Department of Electrical Engineering, University of Louisville, Louisville, Kentucky 40208 U.S.A.*

ABSTRACT   Tension strands are introduced to represent active myocardial fibers. They create one body force proportional to the divergence of the tension-direction vector, and a second equal to the tension divided by the radius of curvature. Explicit solutions to isotropic linearly elastic tensor equations with these body forces are found for the radially-symmetric, linearly-isotropic, elastic spherical heart with arbitrary radial body force. They confirm experiments showing supraluminal intramural pressures. Such pressures may affect coronary perfusion. A tension strand model which is a reasonable compromise between actual myofibrillar geometry and analytical simplicity is the iso-oblique, terminating, nonintersecting model. The body force from that or any other axially symmetric body force can be the forcing term for equations in which the heart is modeled as a thin, ellipsoidal, elastic membrane.

I. INTRODUCTION

The gross mechanical basis for the pumping action of the heart is a difficult and intriguing problem. Because of the inherent difficulty of the subject, many different models can be devised which make one aspect of the problem realistic and which simplify other aspects to the point of tractability. For example, the series and parallel components of force and displacement in the direction of local myocardial fibers can be preserved, and even made nonlinear, if the three-dimensional heart is simplified into a lumped equivalent mechanical model. On the other hand, the three-dimensionality can be realistically preserved and the model simplified by assuming linearity, isotropy, and no systolic forces.

The purpose of this paper is to develop a mechanical model of the heart which is most suitable for investigating how the mechanical stresses and strains in the heart interact with the heart's vascular system in both systole and diastole. This particular application requires that the three-dimensionality of the heart and elastic stresses and strains in all directions be preserved. It requires specific inclusion of the effects of systolic forces. To keep the problem tractable, a linear, isotropic model will be made for the myocardial tissue. Systolic action will be accounted for through the computation and use of body forces arising from tension in the myocardial filaments. To the author's knowledge, the computation and use of such body forces is novel.

II. PREVIOUS RELATED WORK

Elastic Analyses

A number of authors have developed two- or three-dimensional elastic models for a dead or diastolic heart. Mirsky (1974) has provided a recent review of these theories. He states that in

the models the myocardium "acts as a passive medium" and the theories "do not account for muscle contraction." Some of the important such papers include those of Burton (1957), Mirsky (1969, 1973), Sandler and Dodge (1963), Wong and Rautaharju (1968), Hood et al. (1969), Mirsky and Parmley (1973), and Rankin et al. (1977). Kane et al. (1976) add an elastic stability analysis.

One of the special types of three-dimensional analysis is the finite element technique which has been applied to the heart by Gould et al. (1972), Pao et al. (1974), and others. These analyses appear not to involve systolic contractions.

It has long been recognized that a lumped equivalent model for the heart would be useful in describing input/output properties. References to lumped models involving both a myocardial skeleton and contractile elements can be found in Ghista (1974) and Braunwald et al. (1976). This area continues to be active (Good et al., 1974).

Only three approaches have been made which preserve both the three-dimensional aspect of the heart and which specifically include systolic effects. They are those of Streeter et al. (1970), Ghista and Sandler (1969), and the present paper.

Streeter et al. (1970) assumed zero tension orthogonal to myocardial filaments, and only sufficient contractile tensions to satisfy Laplace's law, thereby avoiding an elastic analysis of the heart. There are three possible errors in their formulation: (*a*) There may be extra tension in the middle of the cardiac wall which is offset by compressive elastic forces in the inner wall. (*b*) There may be extra tension in the direction parallel to the myocardial filaments which is offset by negative tension in the orthogonal circumferential direction. (*c*) The use of Laplace's law accounts for radial forces only. Tangential forces arising from the termination of filaments were not included.

Ghista and Sandler (1969) developed a three-dimensional elastic model in which systolic forces were accounted for by introducing a dilation in the strain solution. See also the review by Ghista (1974). Their approach is probably more suited to computations, and less suited to insight, than the present paper. It is not clear to the author whether both radial forces (from filament curvature) and tangential forces (from filament termination) were included in this work.

The present paper handles systolic effects by deriving body forces from the tensions generated, and solves the elastic equations with these body forces. This approach gives more insight than the dilation approach, enabling some new features of the solution to be developed. Since the two methods appear to be complementary, it is desirable to have both available.

Pressure

The natural mathematics for mechanical stresses in the heart is solid mechanics. Pressure is not defined in solid mechanics because there are no equations in which such a definition would appear. Consequently, it is best not to try to borrow a definition of pressure in the heart from the inapplicable field of fluid mechanics, but rather to simply accept that the heart is a solid undergoing tensor stress components for which a single scalar is an inadequate description.

"Intramyocardial pressure" is a term which has become established through previous publications. In this paper this term will be taken generically to mean the study of any or all of the tensor stress components. Following previous usage, it will also be used to mean a specific stress component which is obvious from the context. Most often the stress component implied

will be the component normal to the surface, which for spherical coordinates is the radial component. The normal component is continuous at the surface, which is an important and intuitively-expected property. The other components are not continuous at the surface.

Previous literature relevant to the stress components studied here includes papers which discuss any or all of the three stress components; these authors have not always been precise about either nomenclature or substance. An author, for example, may measure the compressive stress component normal to a surface, compare it (as if it were the same quantity) to another author's measurement with an important contribution tangential to the surface, and call both measurements "intramyocardial pressure." In the review which follows, the original author's nomenclature has been used. Those papers in which it is self-evident which components were actually measured are of course the most valuable papers. Pancake-shaped chambers with flat faces generally parallel to wall edges will contain a hydrostatic pressure generally equal to the stress component normal to the wall. Tunnels will be occluded by the larger of the two stress components normal to the tunnel. The liquids in flexible vessels will likewise be compressed into approximate equilibrium with the larger of the two stress components normal to the vessel. If this changes along the course of the vessel, flow will occur and equilibrium will be a complicated function of the liquid volume enclosed by the vessel, the stresses and mechanical compliances along the vessel and in the vessel wall, and the hydraulic impedance of the cannula-monitor system connected to the vessel. Equilibrium cannot occur, however, at a higher pressure than a stress component normal to some part of the vessel wall. Large spherical chambers will introduce new boundary conditions into the problem and will be difficult to interpret.

Intramyocardial Pressure

Whether intramural pressure can exceed left ventricular pressure has long been recognized as an important question, whose answer is disputable. Johnson and DiPalma (1939) used arteries imbedded in the heart in two pressure measuring nodes, one as an end-terminal of a pressure catheter and the other in an occluding mode. They concluded that peak intramural pressure always exceeds intraluminal pressure. Gregg and Ekstein (1941) repeated these measurements, but performed experiments leading them to believe that experimental artifacts were present. They established that flowing blood impinging upon sensing arteries could create falsely high readings. These were reduced by enclosing the arteries with fenestered covers. They discovered that a fluid-filled space within the beating left ventricle has a pulse pressure which becomes larger than the luminal pulse pressure as the resting pressure in the space is increased. These experiments show that pressures measured in fluid-filled spaces of nonzero resting pressure cannot be considered to equal pressures which would have occurred in the absence of the artificial space, and that all data from fluid-filled spaces of zero resting pressure may not equal undisturbed pressures. They did not offer any explanation for this observed phenomenon, however, even though this might be a significant property of the live heart.

I suspect that these excessive pulse pressures observed by Gregg and Ekstein (1941) may have in fact reflected actual hydrostatic pressures in the experimentally-disturbed myocardium. The law of Laplace would cause the small radii of curvature around the fluid-filled spaces to produce larger pressures for a given wall tension than produced in the lumen with its

larger radii of curvature. It is even possible that a feedback mechanism controlling the strength of contraction near the fluid-filled space was activated to produce higher pulse pressures because of the higher resting pressure.

Salisbury et al. (1962) observed a similar "inotropic" effect on the whole heart squeezed externally by gauze. They used an imbedded arterial catheter and found that the time-course of intramural pressure was M-shaped, with a second and larger peak at the end of systole. This effect was not present in isovolumic contractions. They observed intramyocardial pressures in excess of systolic pressures only below ~45 ml of left ventricular volume.

D'Silva et al. (1963) found a slight supraluminal pressure in some rabbits, and not in others, using a small latex balloon connected to a pressure transducer. They state that their device sometimes produced EKG evidence of infarction, so possibly the device could have produced local myocardial mechanical dysfunction sufficient to raise doubts about whether the measured pressures would have been the same in regions remote from the transducer.

Dieudonne (1967a,b) used a similar device in dog hearts, but obtained an electronically-subtracted difference pressure, which he had taken care to ensure was a true difference in the significant frequency range. His results show that middle-layer, left-ventricle, myocardial pressure exceeds luminal pressure by ~20 mm Hg early in systole, is 15 mm Hg less than luminal pressure late in systole, and has zero difference in mid-systole and in diastole.

Kirk and Honig (1964) used a hollow, curved needle with filed-away notch where local tissue pressure could force local tissue to occlude the path of the fluid flowing through the needle. They found that systolic intramyocardial pressure divided by systolic blood pressure was <1 in the outer part of the myocardium, but exceeded 1.4 in the inner part of the myocardium. They also made a theoretical analysis, which under their assumptions showed that the longitudinal pressures in a cylindrical heart model exceeded the radial pressures. Their Eq. 13 showed that their model had a radial pressure which did not exceed the luminal pressure.

Kirk and Honig (1964) realized that theoretical considerations require that local supraluminal intramyocardial pressures can occur only after the local tissue has contracted. (This is an important point, and will be discussed further in section IV.) They also noted experimental evidence that the supraluminal pressures occur during isovolumic contraction. They reconciled this with the theory by assuming that distortions of the cardiac shape during the isovolumic part of systole allowed the necessary contraction to occur. Their reconciliation may be workable, but I prefer an alternative. Namely, that during the time when the lumen of the ventricle is isovolumic, the heart itself is not, because it is allowing blood stored in the capillaries to flow out through the cardiac veins. The reduced cardiac volume produced by emptying of the capillaries would allow the contraction required by theory.

Baird et al. (1970) used both an occluding artery and an occluding vein with an internal strengthening structure. All their data gave intramural pressures below ventricular pressures. They also repeated the technique of Kirk and Honig (1964) and initially verified their own data. Later runs did show supraluminal pressures, which they attributed to edema. They also pointed out an unaccounted for venturi effect, but did not calculate its magnitude.

Brandi and McGregor (1969) observed intramyocardial pressures only below those of the lumen. They used a constant flow rate into their fluid spaces in the myocardium, presumably

because the injected fluid was leaking somewhere. The leakage may affect the validity of their conclusions.

van der Meer et al. (1970) used an imbedded segment of vein operating in a flow-occluding mode. They found that systolic intramyocardial pressure exceeded ventricular pressure by up to 50%. They also discovered that a large artery as transducer gave different results from those of a small vein. In addition to properties of the vessel used, they suspected effects of trauma to the myocardium.

Armour and Randall (1971) used a small pressure transducer imbedded in the myocardial wall. They found that peak deep intramyocardial pressure exceeded luminal pressure by about one-fifth. They also noted that epicardial intramyocardial pressure rose before deep pressure. (The latter is interesting because the depolarization wave of the action potential goes from endocardium to epicardium.) I infer that Armour and Randall (1971) used hydrostatic pressure to calibrate their device. The transducer's location and structure may have tended to measure mostly radial pressure σ_r upon two opposite sides only. Since they do not report calibrating the device with lateral force, the exact significance of their data is uncertain. Their lead II EKG showed slight ST elevation and gross T-wave inversion, which suggests that their device may have produced local ischemic changes in the myocardium.

Gregg (1950, Fig. 45), showed that a ligated coronary vein had a substantial excess of pressure over that of the aorta. An experiment by Pifarre (1968) showed that a vein graph originating in the aorta and implanted into the left ventricular wall had from 60 to 100 mm Hg more peak pressure than the aorta. Backflow through the graph was prevented by a functioning valve in the implanted vein segment. These two experiments are important because the measurement of a hydraulic pressure in blood is much less subject to artifactual error than measurements in a moving solid undergoing tensor stresses.

Archie (1975) has offered a theoretical analysis in which supraluminal pressures were inferred from a constant-resistance, no-capitance model of coronary blood flow. His analysis may be incorrect because of capacitive effects of the large capillary bed, which expands substantially in diastole (Tillmanns et al., 1974).

The analysis in section IV of this paper appears to be the first to solve a stress-strain model which produces a radial pressure component exceeding luminal pressure, the second (after Kirk and Honig, 1964) to produce a tangential pressure component exceeding the luminal pressure, and the first to use a noncylindrical model to conclude that both orthogonal tangential components of pressure exceed luminal pressure.

III. GENERAL TENSION STRANDS AND THEIR BODY FORCES

Conceptual Context for Myocardial Body Forces

In the classical mechanics of elastic media, provision is made for electrostatic, electromagnetic, gravitational, and Coriolis forces which act upon the substance of the elastic medium. These are called body forces, and provision is made for their inclusion when the sum of all the forces upon a differential body element is equated to zero.

In this paper, the effect of the contraction of a muscle strand will be derived to be some new term which enters the differential equations in the same place as a traditional body force. The

mathematical structure of how a term enters the differential equations is more important than traditional limitations upon the physical origin of these forces, so the new forces will also be called body forces.

Symbols for Section III

A_i, B_i — Spatial position of the ends of the ith tension strand.

dA — Elemental area normal to continuous tension strands.

$F(r)$ — Total body force density for continuous tension strands.

F_{accel} — Acceleration body force created by curvature of continuous tension strands.

F_{term} — Terminal body force for continuous tension strands.

$l_i(0)$ — Unit vector in strand direction at the A_i terminal of a discrete tension strand.

$l_i(1)$ — Unit vector in strand direction at the B_i terminal of a discrete tension strand.

L_i — Length of ith discrete tension strand.

p — Vector such that dp is an incremental vector in the $s(r)$ direction.

$q_i(\ )$ — Fractional distance along discrete tension strand.

$\hat{q}_i(0), \hat{q}_i(1)$ — The unit directions of the terminal forces of a discrete tension strand at A_i and B_i, respectively.

r — Vector position in myocardium.

$s(r)$ — Direction of continuous tension strands at point r.

τ_i — Peak tension in the ith discrete tension strand.

$\tau(r)$ — Peak tension per area normal to direction of continuous tension strands at position r.

α — Fractional distance along discrete tension, zero at A_i end.

δ — Infinitesimal operator.

$\delta(\ )$ — Three-dimensional Dirac delta function.

ρ — Radius of great circle followed by $s(r)$.

τ — Cardiac cycle variable, 0 in diastole and 1 in full systole.

Discrete Simple Tension Strands

Assume that the myocardial contractile elements develop a set of forces which can be represented as follows. The ith such element begins in location (before displacement) A_i, has tension $\tau\ T_i$, ($\tau = 0$ in diastole, $\tau = 1$ in full systole), has length L_i, and travels along path
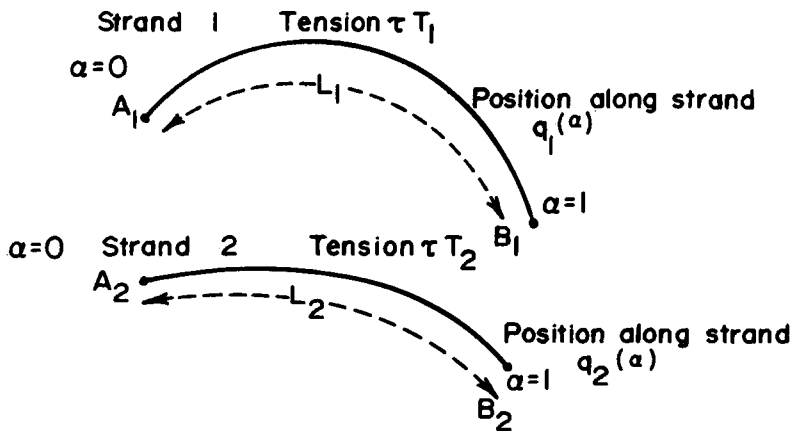

FIGURE 1 Geometric definitions for discrete tension strands. Strand 1 begins (for $\alpha = 0$) at position A_1, has an arc length L_1 and position $q_1(\alpha)$ at the fractional position α along the arc, and ends at B_1 (where $\alpha = 1$).

$q_i(\alpha)$, where α is a scalar length which varies between 0 and L_i and $q_i(\alpha)$ is a vector function of this scalar. The ith tension strand is assumed to end at B_i, so that $q_i(0) = A_i$ and $q_i(L_i) = B_i$. The function $q_i(\alpha)$ will be assumed to have three bounded derivatives with respect to α. The geometry is illustrated in Fig. 1. The tension strand represents the active part of a myocardial cell. It will be assumed that there are no tangential forces exerted by the tension strand, but normal and end forces will be allowed.

There will be two types of body force developed by the ith such contractile element. One type will be forces at the end points A_i and B_i. (When the path is closed loop, however, A_i will equal B_i and there will be no end-point force.) The second type of force will be due to accelerations in $q_i(\alpha)$.

The acceleration force on the interval $q_i(\alpha - \delta\alpha)$ to $q_i(\alpha + \delta\alpha)$ can be found by considering the tension at $q_i(\alpha - \delta\alpha)$ to be in the unit direction $-dq_i(\alpha - \delta\alpha)/d\alpha$ and the tension at $q_i(\alpha + \delta\alpha)$ to be in the unit direction $dq_i(\alpha + \delta\alpha)/d\alpha$. Evaluating $dq_i(\alpha \pm \delta\alpha)/d\alpha$ by a two-term Taylor series, noting that the length of the segment is $2\delta\alpha L_i$, and using the fact that the sum of the end forces gives the net force of the tension strand upon the medium gives

$$\tau T_i \frac{d^2 q_i(\alpha)}{d\alpha^2} \tag{3-1}$$

for the acceleration force per length.

The unit direction of the terminal force at A_i is

$$\frac{dl_i(\alpha)}{d\alpha} \left| \frac{dl_i(\alpha)}{d\alpha} \right|^{-1} \equiv \hat{l}_i(\alpha) \tag{3-2}$$

evaluated at $\alpha = 0$, while the direction of the terminal force at B_i will be the negative of the above evaluated at $\alpha = L_i$.

The total force density will therefore be

$$F(r) = \sum_{\text{all } i} \tau T_i \left\{ \hat{l}_i(0)\delta(r - A_i) - \hat{l}_i(L_i)\delta(r - B_i) + \int_0^{L_i} \frac{d^2 l_i(\alpha)}{d\alpha^2} \delta[r - l_i(\alpha)]d\alpha \right\}, \tag{3-3}$$

where δ denotes the Dirac delta function of three-dimensional argument. In the above, note that T_i is assumed to be an independent variable which does not depend upon the displaced positions and lengths, and L_i is the length of the ith strand after any displacement may have occurred.

Continuous Simple Tension Strands

Simple tension strands will be defined to be tension strands which do not cross each other, except at isolated singular points. Let the direction of the tension strands at point r be the unit magnitude vector $s(r)$, which may be defined to be positive in either of the two opposite directions in which the strands run. Let the force in a differential area dA normal to $s(r)$ be $\tau T(r) \, dA$. The magnitude of the density of the terminal body force will be the divergence of the tension-direction product. The direction will be $-s(r)$ if the divergence is positive, and $s(r)$ if the divergence is negative. In both cases the terminal force density will be

$$\mathbf{F}_{\text{term}} = s(r) \text{ div } [\tau T(r) \, s(r)]. \tag{3-4}$$

The acceleration force per volume at $\mathbf{r}$ will be

$$\mathbf{F}_{accel} = \tau T(\mathbf{r}) \frac{d^2 \mathbf{s}(\mathbf{r})}{d\mathbf{p}^2}, \qquad (3\text{-}5)$$

where $d\mathbf{p}$ is in the $\mathbf{s}(\mathbf{r})$ direction. If $\mathbf{s}(\mathbf{r})$ were a great circle on a spherical surface of radius ρ, then the above force density would have magnitude

$$\frac{\tau T(\mathbf{r})}{\rho} \qquad (3\text{-}6)$$

and would be directed toward the center of the sphere. Combining the terminal and acceleration force densities gives

$$\mathbf{F}(\mathbf{r}) = -\mathbf{s}(\mathbf{r}) \, \mathrm{div} \, [\tau T(\mathbf{r})] + \tau T(\mathbf{r}) \frac{d^2 \mathbf{s}(\mathbf{r})}{d\mathbf{p}^2}. \qquad (3\text{-}7)$$

Comments

The preceding approach could be extended by considering the T_i of the discrete analysis or the $T(\mathbf{r})$ of the continuous analysis to be the sum of a contractile tension and an elastic tension. The elastic tension could be an appropriate dependent function of length and the contractile history.

The deductive exposition here begins with assumed known tensions, and infers body forces. The inductive problem of working from forces to tension strands is not well understood. As pointed out in section II, Laplace's law alone cannot provide uniqueness to the inductive problem without invoking arbitrary assumptions which may or may not be reasonable. Integrating both the terminal and acceleration forces in the inductive problem is especially difficult. Streeter et al. (1970) apparently avoided this difficulty by not including the terminal forces. Since the terminal body forces are circumferential rather than radial, this omission may not be serious.

IV. A SYMMETRICAL, SPHERICAL HEART WITH BODY FORCES

The following heart model will be analyzed in this section: (a) The heart is assumed to be a thick spherical shell of inner radius r_1 and outer radius r_0. (b) The body forces are radially symmetric and directed toward the center of the heart. (c) The heart consists of an elastic skeleton which is linear and isotropic, upon which body forces (generated by contractile tensions) are applied. (d) The heart will be analyzed under conditions of static equilibrium, so that inertial forces are ignored.

Each of these assumptions is only a rough approximation to an actual heart ventricle, and better simplifications could be made. Unfortunately, their mathematical solution would be extremely difficult, and would tend to obscure some important qualitative points which can be better made with a simple model. The simple model outlined above will be analyzed in this section to develop insight into the biophysical phenomena involved.

Symbols for Section IV

    a_i Maximum body force coefficient of r^i (see Eq. 4-1).

    $A, \hat{B}$ Respective arbitrary coefficients of $\hat{r}$ and $\hat{r}^{-2}$ in homogeneous solution.

e_r, e_θ, e_ϕ	Unit vectors in respective dr, $d\theta$, $d\phi$ spherical coordinate directions.
$\hat{f}(\hat{r})$	Forced solution for $\hat{U}(\hat{r})$ given by Eq. 4-5.
$\hat{g}(\hat{r})$	Forced solution for $\sigma_{rr}(\hat{r})$ given by Eq. 4-8.
$\hat{h}(\hat{r})$	Forced solution for $\sigma_{cc}(\hat{r})$ given by Eq. 4-12b.
K	Hydraulic compliance of systemic arterial system, having units of volume per pressure.
P	Left ventricular luminal pressure.
P_0, P_1	Respective outer and inner pressures on left ventricle.
$P_{\text{iso }V}$	Luminal pressure under isovolumic contraction.
Q	Function defined by Eq. 4-17a.
r	Radial position, units of length.
$\hat{r}$	Normalized radial position, $\hat{r} = r/r_1$.
r_0, r_1	Respective outer and inner radii of spherical left ventricle.
R	Radial body force per mass ($\hat{R} = R$).
$U(r)$	Radial position of heart location initially at radius r before contraction, units of length.
$\hat{U}(\hat{r})$	Normalized radial position of heart location initially at radius of $\hat{r}$ before contraction, $\hat{U}(\hat{r}) = U(r/r_1)/r_1$, no units.
V	Left ventricular stroke volume.
$V_{\text{stroke } P_1 = 0}$	Left ventricular stroke volume when aortic pressure is zero.
W	Function defined by Eq. 4-17b.
γ	Constant defined by Eq. 4-15a.
δ	Small increment, also defined by $\nu = 1 + \delta$.
ϵ	Constant defined by Eq. 4-15c.
θ	Spherical coordinate.
K	Constant defined by Eq. 4-15b.
λ	Elastic constant of myocardium.
μ	Elastic constant of myocardium.
ν	Ratio of outer to inner left ventricular radii, r_0/r_1.
π	3.1416.
ρ	Specific gravity of myocardium.
$\sigma_{rr}, \sigma_{\theta\theta}, \sigma_{\phi\phi}, \sigma_{cc}$	Compressive stress components, where c denotes any circumferential direction.
τ	Cardiac cycle variable, 0 in diastole and 1 in full systole.
ϕ	Spherical coordinate.

Notation

Spherical coordinates r, θ, and ϕ will be used, centered at the center of a heart which is a shell bounded by two spheres of radius r_1 and r_0, with $r_1 < r_0$. If the radial coordinate of position of an unstressed point in the heart is r, then its position after stress will be in the same radial direction at radius $U(r)$. The stress components will be σ_{rr}, $\sigma_{\theta\theta}$, $\sigma_{\phi\phi}$, $\sigma_{r\theta}$, $\sigma_{r\phi}$, and $\sigma_{\theta\phi}$. The unit direction vectors in the r, θ, and ϕ directions will be denoted by e_r, e_θ, and e_ϕ. Normalized variables will be used, defined by $\hat{r} = r/r_1$, $\hat{U}(\hat{r}) = U(r)/r_1$. λ and μ are the usual isotropic elastic constants (Love, 1927). The tension strands will be assumed to be a set of symmetric, randomly-oriented great circles, resembling the windings of a golf-ball core. Eq. 3-7, by the assumed symmetry, will reduce to a general radial body force which can be defined to be the power series

$$\rho R = -\tau \sum_i a_i r^i \tag{4-1}$$

$$\rho R = \rho \hat{R} = -\tau \sum_i \hat{a}_i \hat{r}^i, \tag{4-2}$$

where ρ is the mass per volume, and $\hat{a}_i = a_i r_1^i$. It is convenient, but not necessary, to think of i as having integer values.

General Solution

Love (1927) has shown that the general equation for static equilibrium under this model is

$$(\lambda + 2\mu) \frac{\partial}{\partial r} \left[\frac{\partial U(r)}{\partial r} + 2 \frac{U(r)}{r} \right] + \rho R = 0 . \qquad (4\text{-}3)$$

The normalized version of this equation is the same with U, r, and R replaced by $\hat{U}$, $\hat{r}$, $\hat{R}$, respectively. The general solution to this equation is the forced solution plus the homogeneous solution. It is easily verified that the homogeneous solution is $\hat{U}_{\text{homo}} = \hat{A}\hat{r} + \hat{B}\hat{r}^{-2}$. The forced solution to $\rho\hat{R} = -\tau \hat{a}_i \hat{r}^i$ can be found by assuming that it is an unknown constant times an unknown power of $\hat{r}$. The resulting formula gives the homogeneous solution when i equals -1 or -4, in which case the forced solution is a constant times a power of $\hat{r}$ times $\ln \hat{r}$. The general solution can be written compactly as

$$\hat{u} = [\hat{r}, \hat{r}^{-2}] \begin{bmatrix} \hat{A} \\ \hat{B} \end{bmatrix} + \hat{f}(\hat{r}), \qquad (4\text{-}4)$$

where

$$\hat{f}(\hat{r}) = \frac{\tau \hat{a}_{-1} \hat{r} \ln \hat{r}}{3(\lambda + 2\mu)} - \frac{\tau \hat{a}_{-4} \ln \hat{r}}{3\hat{r}^2(\lambda + 2\mu)} + \sum_{\substack{i \\ i \neq -1, -4}} \frac{\tau \hat{a}_i \hat{r}^{i+2}}{(\lambda + 2\mu)(i + 1)(i + 4)} . \qquad (4\text{-}5)$$

The radial stress σ_{rr} is given by (Love, p. 142)

$$\sigma_{rr} = (\lambda + 2\mu) \frac{\partial u}{\partial r} + 2\lambda \frac{u}{r} . \qquad (4\text{-}6)$$

Note that $\hat{U}$ and $\hat{r}$ can replace U and r, respectively. Substituting Eqs. 4-4 and 4-5 in 4-6, carrying out the differentiations, and rearranging gives

$$\sigma_{rr}(\hat{r}) = [1, \hat{r}^{-3}] \begin{bmatrix} 3\lambda + 2\mu, 0 \\ 0, -4\mu \end{bmatrix} \begin{bmatrix} \hat{A} \\ \hat{B} \end{bmatrix} + \hat{g}(\hat{r}), \qquad (4\text{-}7)$$

where

$$\hat{g}(\hat{r}) = (\lambda + 2\mu) f'(\hat{r}) + \frac{2\lambda \hat{f}(\hat{r})}{\hat{r}} . \qquad (4\text{-}8)$$

Let $r_0/r_1 = \nu$. Note that $\nu > 1$. Equating $\sigma_{rr}(r_1)$ to $-P_1$ and $\sigma_{rr}(r_0)$ to $-P_0$ gives the matrix equation

$$\begin{bmatrix} -P_0 \\ -P_1 \end{bmatrix} = \begin{bmatrix} 1, -\nu^{-3} \\ 1, 1 \end{bmatrix} \begin{bmatrix} 3\lambda + 2\mu, 0 \\ 0, -4\mu \end{bmatrix} \begin{bmatrix} \hat{A} \\ \hat{B} \end{bmatrix} + \begin{bmatrix} \hat{g}(\nu) \\ \hat{g}(1) \end{bmatrix} . \qquad (4\text{-}9)$$

Solving for the vector of $\hat{A}$ over $\hat{B}$, and substituting in Eqs. 4-7 and 4-4 gives

$$\sigma_{rr}(\hat{r}) = \frac{[1, \hat{r}^{-3}]}{\nu^3 - 1} \begin{bmatrix} -\nu^3, & 1 \\ \nu^3, & -\nu^3 \end{bmatrix} \begin{bmatrix} P_0 + \hat{g}(\nu) \\ P_1 + \hat{g}(1) \end{bmatrix} + \hat{g}(\hat{r}) \tag{4-10}$$

$$\hat{u}(\hat{r}) = \frac{[\hat{r}, \hat{r}^{-2}]}{\nu^3 - 1} \begin{bmatrix} \dfrac{-\nu^3}{3\lambda + 2\mu}, & \dfrac{1}{3\lambda + 2\mu} \\[2mm] \dfrac{-\nu^3}{4\mu}, & \dfrac{\nu^3}{4\mu} \end{bmatrix} \begin{bmatrix} P_0 + \hat{g}(\nu) \\ P_1 + \hat{g}(1) \end{bmatrix} + \hat{f}(\hat{r}). \tag{4-11}$$

The circumferential tension $\sigma_{\theta\theta} = \sigma_{\phi\phi} = \sigma_{cc}$ equals $\lambda \partial U/\partial r + 2(\lambda + \mu)U/r$ (Love, p. 142). This evaluates to

$$\sigma_{cc} = \frac{[1, \hat{r}^{-3}]}{\nu^3 - 1} \begin{bmatrix} -\nu^3, & 1 \\[1mm] \dfrac{\nu^3}{2}, & \dfrac{-\nu^3}{2} \end{bmatrix} \begin{bmatrix} P_0 + \hat{g}(\nu) \\ P_1 + \hat{g}(1) \end{bmatrix} + \hat{h}(\hat{r}) \tag{4-12a}$$

where

$$\hat{h}(\hat{r}) = \lambda f'(\hat{r}) + 2(\lambda + u)\hat{f}(\hat{r})\hat{r}^{-1}. \tag{4-12b}$$

The transient solution, in which $\hat{g}(\hat{r}) = 0$ and $\hat{f}(\hat{r}) = 0$, is well known (Love, 1927). When $P_1 > 0$ and $P_0 = 0$, the transient begins at its maximum at $\hat{r} = 1$ and decreases monotonically to zero.

Single Power Forced Solution

If $\rho\hat{R} = -\hat{a}_i\hat{r}^i$ where i is any integer or fraction except -1 or -4, then the forced solution for σ_{rr} can be evaluated, as follows. Eqs. 4-5 and 4-8 give

$$\hat{f}(\hat{r}) = \hat{a}_i\gamma\hat{r}^{i+2} \tag{4-13}$$

$$\hat{g}(\hat{r}) = \hat{a}_i\epsilon\hat{r}^{i+1}, \quad \hat{h}(\hat{r}) = \hat{a}_i\kappa\hat{r}^{i+1} \tag{4-14}$$

where

$$\gamma = \tau[(\lambda + 2\mu)(i + 1)(i + 4)]^{-1} \tag{4-15a}$$

$$\kappa = \lambda\gamma(i + 2) + 2(\lambda + \mu)\gamma \tag{4-15b}$$

$$\epsilon = \frac{\tau}{(i + 1)(i + 4)}\left[i + 2 + \frac{2\lambda}{\lambda + 2\mu}\right]. \tag{4-15c}$$

If it is assumed that $P_0 = 0$, then substitution of Eq. 4-14 into 4-10, and 4-12 and separation of the terms multiplied by P_1 from those multiplied by $\hat{a}_i$ lead to the following:

$$(\nu^3 - 1)\sigma_{rr}(\hat{r}) = P_1[1 - \nu^3\hat{r}^{-3}] + \hat{a}_i\epsilon Q(\hat{r}, \nu, i) \tag{4-16a}$$

$$(\nu^3 - 1)\sigma_{cc}(\hat{r}) = P_1[1 - 0.5\nu^3\hat{r}^{-3}] + \hat{a}_iW(\hat{r}, \nu, i), \tag{4-16b}$$

where

$$Q(\hat{r}, \nu, i) = 1 - \nu^4 + \hat{r}^{-3}(\nu^{i+4} - \nu^3) + \hat{r}^{i+1}(\nu^3 - 1) \tag{4-17a}$$

$$W(\hat{r}, \nu, i) = \epsilon[1 - \nu^{i+4} + 0.5\hat{r}^{-3}(\nu^{i+4} - \nu^3)] + \kappa\hat{r}^{i+1}(\nu^3 - 1). \tag{4-17b}$$

The bracketed terms in (4-16a) and (4-16b) are proportional to the previously-known homogeneous solution. The $Q(\hat{r}, \nu, i)$ and $W(\hat{r}, \nu, i)$ terms in (4-16a) and (4-16b) are of special interest because they are new and because they may produce supraluminal stresses. Direct evaluation shows that

$$Q(1, \nu, i) = 0 = Q(\nu, \nu, i) \tag{4-18}$$

$$\frac{\partial Q(\hat{r}, \nu, i)}{\partial \hat{r}} = -3\hat{r}^{-4}(\nu^{i+4} - \nu^3) + (i + 1)\hat{r}^i(\nu^3 - 1) \tag{4-19}$$

$$\frac{\partial^2 Q(\hat{r}, \nu, i)}{\partial \hat{r}^2} = [12\hat{r}^{-5}(\nu^{i+4} - \nu^3)] + [i(i + 1)\hat{r}^{i-1}(\nu^3 - 1)]. \tag{4-20}$$

If $i \geq 0$, the first bracketed term in (4-20) is positive, and the second is nonnegative, so that the second derivative is positive. Consequently, for $i \geq 0$, $Q(\hat{r}, \nu, i)$ starts at 0 for $\hat{r} = 1$, descends to a unique minimum somewhere in the interval $1 < \hat{r} < \nu$, and then rises to 0 at $\hat{r} = \nu$. If the radial pressure is defined as $-\sigma_{rr}(\hat{r})$, then the radial pressure of the forced solution starts at zero at $\hat{r} = 1$, rises to a unique maximum somewhere in the interval, and then falls to zero at $\hat{r} = \nu$. Equating the derivative, Eq. 4-19, to zero and solving gives

$$\hat{r}_{\text{forced peak}} = \left[\frac{3(\nu^{i+4} - \nu^3)}{(i + 1)(\nu^3 - 1)}\right]^{1/(4+i)} \tag{4-21}$$

$$Q_{\min}(\hat{r}_{\text{forced peak}}, \nu, i) = 1 - \nu^4 + \left[\frac{(i + 1)(\nu^3 - 1)}{3(\nu^{i+4} - \nu^3)}\right]^{3/(i+4)}$$

$$\cdot (\nu^{i+4} - \nu^3) + \left[\frac{3(\nu^{i+4} - \nu^3)}{(i + 1)(\nu^3 - 1)}\right]^{(i+1)/(i+4)} (\nu^3 - 1). \tag{4-22}$$

The special case of constant force per mass, given by $i = 0$, gives

$$\hat{r}_{\text{forced peak}} = \left[\frac{3(\nu^4 - \nu^3)}{\nu^3 - 1}\right]^{1/4}$$

$$Q_{\min}(\hat{r}_{\text{forced peak}}, \nu, 0) = 1 - \nu^4 + \left[\frac{\nu^3 - 1}{3(\nu^4 - \nu^3)}\right]^{3/4}(\nu^4 - \nu^3) + \left[\frac{3(\nu^4 - \nu^3)}{\nu^3 - 1}\right]^{1/4}(\nu^3 - 1). \tag{4-23}$$

Further simplification can be made by assuming that $\nu = 1 + \delta$, where $\delta \ll 1$, so that

$$\hat{r}_{\text{forced peak}} \simeq 1 + \frac{\delta}{2} \tag{4-24}$$

$$Q\left(1 + \frac{\delta}{2}, 1 + \delta, 0\right) = \frac{-3\delta^3}{2} + \text{terms of order } \delta^4 \tag{4-25}$$

$$\sigma_{rr}\left(1 + \frac{\delta}{2}\right) = \frac{1}{3\delta + 3\delta^2 + \delta^4}\left\{P_1\left[\frac{-3\delta^3}{2} + \text{terms of order } \delta^2\right]\right.$$

$$\left. + \hat{a}_i\epsilon\left[\frac{-3\delta^3}{2} + \text{terms of order } \delta^4\right]\right\}. \quad (4\text{-}26)$$

Note that the forced term will be about twice the homogeneous term at $\hat{r} = 1 + \delta/2$ provided that

$$\hat{a}_i = \frac{2P_1}{\epsilon\delta^2}. \quad (4\text{-}27)$$

The important qualitative conclusion from this analysis is that so long as $Q(\hat{r}, \nu, i)$ is negative (for which nonnegative i is a sufficient condition) then the forced solution for $-\sigma_{rr}$ can be arbitrarily large if $\hat{a}_i$ becomes large enough, which simply means that the body force is large enough.

Single Power Incompressible Solutions

For incompressible tissues, λ is infinite, which implies that $\gamma = 0, \hat{f}(\hat{r}) = 0, \kappa = \tau/(i + 1) = \epsilon$, $\hat{g}(\hat{r}) = \hat{a}_i\tau r^{i+1}(i + 1)^{-1} = \hat{h}(\hat{r})$. Therefore,

$$\sigma_{rr} = \frac{[1, \hat{r}^{-3}]}{(\nu^3 - 1)}\begin{bmatrix} -\nu^3, 1 \\ \nu^3, -\nu^3 \end{bmatrix}\begin{bmatrix} P_0 + \hat{a}_i\tau\nu^{i+1}(i + 1)^{-1} \\ P_1 + \hat{a}_i\tau(i + 1)^{-1} \end{bmatrix} + \hat{a}_i\tau\hat{r}^{i+1}(i + 1)^{-1} \quad (4\text{-}28)$$

$$\sigma_{cc} = \frac{[1, \hat{r}^{-3}]}{\nu^3 - 1}\begin{bmatrix} -\nu^3, 1 \\ \dfrac{\nu^3}{2}, \dfrac{-\nu^3}{2} \end{bmatrix}\begin{bmatrix} P_0 + \hat{a}_i\tau\nu^{i+1}(i + 1)^{-1} \\ P_1 + \hat{a}_i\tau(i + 1)^{-1} \end{bmatrix} + \hat{a}_i\tau\hat{r}^{i+1}(i + 1)^{-1} \quad (4\text{-}29)$$

$$\hat{u}(\hat{r}) = \frac{\nu^3}{4\mu\hat{r}(\nu^3 - 1)}[P_1 - P_0 - \hat{a}_i\tau(i + 1)^{-1}(\nu^{i+1} - 1)]. \quad (4\text{-}30)$$

Figs. 2 and 3 are plots of Eqs. 4-28 and 4-29 for $P_0 = 0$, $P_1 = 100$ mm Hg, $i = 0$, and $\nu = 1.3$. Eq. 4-30 shows that there is no displacement for $\hat{a}_0\tau = 333\frac{1}{3}$, but that there is inward displacement for larger values of $\hat{a}_0\tau$. Note that values of $\hat{a}_0\tau$ less than $333\frac{1}{3}$ would not be sufficient to generate 100 mm Hg of pressure, while larger values generate a contraction such that compressive forces resisting the contraction resist part of the applied body force. These figures clearly illustrate that theoretical possibility of intramural pressures exceeding luminal pressures after systolic ejection has begun. Nothing in this paper or in the references cited suggests that supraluminal pressures are created by passive filling of the heart.

Pressure and Volume Performance of Systolic Elastic
Radially Symmetric Hearts

It has been well known to engineers and physicists that the two-terminal, current-voltage properties of a linear device can be fully characterized by the open-circuit voltage and the closed-circuit current. From this data, both Thévenin and Norton equivalent circuits can be established. If the heart is to be analyzed on a beat-by-beat basis, then the appropriate analogs of the open-circuit voltage is the isovolumic pressure, and the appropriate analog of the
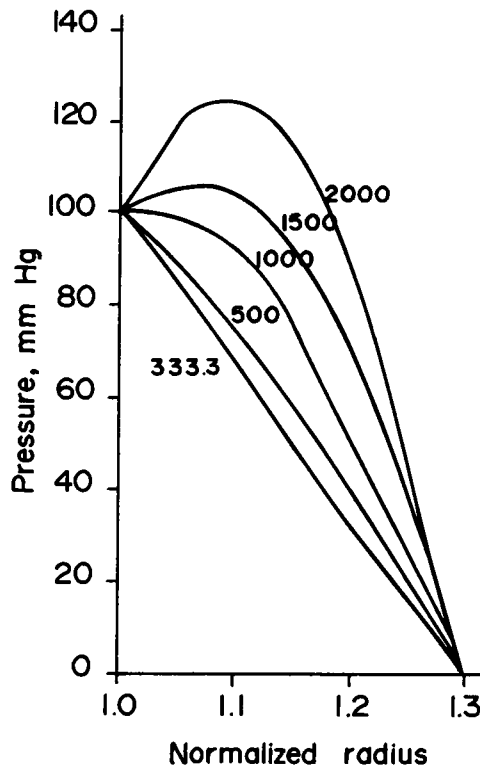
FIGURE 2   Radial stress, $-\sigma_{rr}$, in the thick radially-symmetric, concentric, spherical, linearly-elastic, heart model with radially-symmetric constant body forces. The normalized body force is the labeled value at $\hat{a}_0 r$. Note that because of the active systolic force, there is no unique radial stress for a given luminal pressure. The higher body forces in the tissue have created compressive stresses in the inner layers of the heart model.

short-circuit current is the volume pumped out in the heart if the heart were emptying into an aorta at zero pressure. The isovolumic pressure and zero-pressure stroke volume would completely characterize the output of a linear elastic heart. The purpose of this subsection is to derive expressions of these parameters for a spherical, linearly elastic heart with a radially symmetric body force which follows a power law.

In solving for the isovolumic pressure, the interior pressure is a dependent variable. It is defined as that pressure for which the displacement at the interior radius is equal to zero. Assuming P_0 is a known independent variable, and equating $\hat{U}(1)$ in Eq. (4-11) to zero and solving for P_1 gives the equation

$$P_{(1\ iso\ \nu)} = \{\nu^3 4\mu[P_0 + \hat{g}(\nu)] - \hat{g}(1)4\mu + \nu^3(3\lambda + 4\mu)[P_0 + \hat{g}(\nu)] - \nu^3\hat{g}(\nu)$$
$$\cdot (3\lambda + 4\mu) - \tau\hat{f}(1)(\nu^3 - 1)(3\lambda + 2\mu)4\mu\}[4\mu + \nu^3(3\lambda + 2\mu)]^{-1}. \quad (4\text{-}31)$$

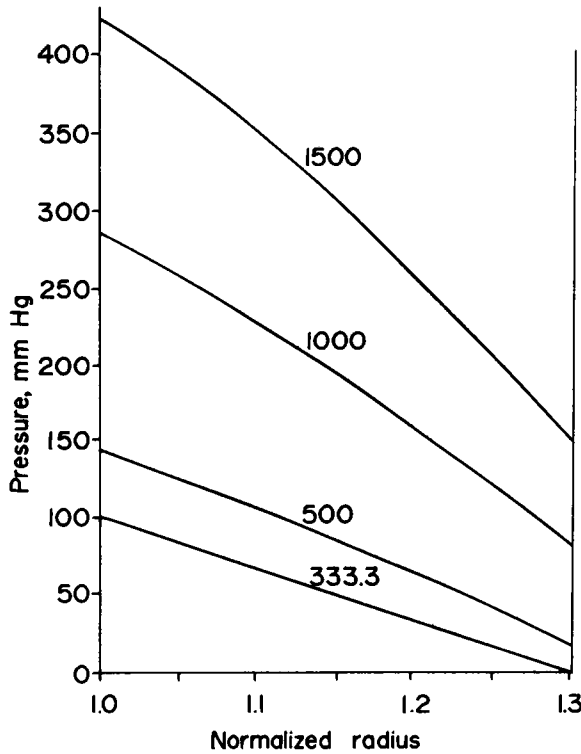The stroke volume at zero pressure is $(4\pi r_1^3/3)[1 - \hat{U}(1)]$, where $P_1 = 0$. The solution is

FIGURE 3 Circumferential stress, σ_{cc}, in the thick, radially-symmetric, concentric, spherical, linearly-elastic heart model with constant radially-symmetric body force, labeled as $\hat{a}_0 r$.

$$V_{(\text{stroke } P_1-0)} = \frac{4\pi r_1^3}{3}\left\{ 1 + \frac{\nu^3(P_0 + \hat{g}(\nu))}{(3\lambda + 2\mu)(\nu^3 - 1)} - \frac{P_1\hat{g}(1)}{(3\lambda + 2\mu)(\nu^3 - 1)} + \frac{\nu^3(P_0 + \hat{g}(\nu))}{4\mu(\nu^3 - 1)} \right.$$
$$\left. - \frac{\nu^3[P_1 + \hat{g}(1)]}{4\mu(\nu^3\ 1)} - \tau\hat{f}(1) \right\}. \quad (4\text{-}32)$$

If the heart were to beat into a compliance of K, then the pressure developed would follow the simultaneous solution of

$$V/P = K \quad (4\text{-}33)$$

and

$$\frac{V_{(\text{stroke } P_1-0)} - V}{P} = \frac{V_{(\text{stroke } P_1-0)}}{P_{1\ \text{iso}-V)}}. \quad (4\text{-}34)$$

This is analogous to crossing the equation for an external resistance with the electrical "load line" of the source. The solution occurs at

$$P = \frac{P_{(1\ \text{iso}-V)}V_{(\text{stroke } P_1-0)}}{V_{(\text{stroke } P_1-0)} + P_{(1\ \text{iso}-V)}K} \quad (4\text{-}35)$$

$$V = \frac{P_{(1\ iso-V)} V_{(stroke\ P_1-0)} K}{V_{(stroke\ P_1-0)} + P_{(1\ iso\ V)} K}$$ (4-36)

The complexity of the formulas for $V_{(stroke\ P_1-0)}$ and $P_{(1\ iso-V)}$ should not be allowed to confuse what is a simple conceptual situation. The myofibrillar strands create linear tensions which produce body forces. If the heart is found to work isovolumically, when it is initially full of blood at zero pressure, these body forces will cause intraluminal pressure to rise to $P_{(1\ iso-V)}$. Elastic stresses will always occur in the myocardial wall at this time. Elastic strains (distortions) will occur in the outer heart wall, unless the heart is incompressible. (Elastic incompressibility with finite shearability implies $K = \infty$, $\lambda = \infty$, μ finite, $E = 3\mu$, and $\sigma = \frac{1}{2}$.) If the heart is incompressible, then no elastic distortions (strains) will occur; if it is compressible, then elastic distortions will occur. If a finite blood volume is allowed to leave the ventricular chamber, the given body forces will not develop the full $P_{(1\ iso-V)}$ of which they are capable, but will place the endocardial part of the elastic myocardial skeleton under compressive forces. Laplace's law, $\Delta P = T/R$, can be applied to such a heart in systole, but the tensions calculated by the law will be the sum of the contractile tensions and the elastic tensions. Thus, both a dead heart and a live systolic heart could be filled to 100 mm Hg in the ventricular lumen, and both would have the same total pressure tensions. The difference would be that the dead heart would have zero contractile tensions, while the live systolic heart would have nonzero contractile tension. It would have zero elastic tension, or positive compressive elastic tension, if it had pumped no or some blood, respectively. Laplace's law, quite clearly, gives information only on the sum of contractile and elastic tensions. Additional information not available in Laplace's law must be used to determine which of the infinite configurations of contractile and elastic strains is actually present.

V. ELLIPSOIDAL GEOMETRY

The purpose of this section is to define parameters for an ellipsoid of revolution. This geometry will be used in the next two sections.

Symbols for Sections V, VI, VIII

a	Minor radius of ellipse.
dA	Surface element, element of cross sectional area.
b	Major radius of ellipse and axis of rotation.
e_ϕ, e_β, e_θ, e_ζ	Unit vectors defined in Fig. 5.
F_a	Tension per cross sectional area of continuous strands tension per length in surface normal to strand direction.
g_ϕ, g_θ	See Eqs. 5-5 and 5-6.
h	Shell thickness of heart.
K	Elastic constant.
N_ϕ, N_θ	Planar elastic stresses obtained by integrating over heart wall thickness by Eqs. 7-3 and 7-4.
p	Position on ellipsoidal surface.
q_ϕ, q_ζ	Components of total force density (systolic body forces plus pressure forces) per area of middle surface.
$r(\phi)$	Distance from ellipse surface to axis of revolution.
R_ϕ, R_θ	See text between Eqs. 5-1 and 5-2.
u, u_ϕ, u_ζ	Incremental displacement vector of point in myocardial middle surface and its components.

x Cartesian coordinate, minor axis generating ellipse.
y Cartesian coordinate, major axis generating ellipse.
β Angle between tension strands and myocardial equator.
θ Elliptical coordinate (Fig. 4).
μ Elastic constant.
π 3.1416.
ϕ Elliptical coordinate (Fig. 4).
$\overline{N}_{\phi 0}, \overline{N}_{\pi/2}$ Number of strands crossing surface of given by ϕ equal to the subscripted value.
γ Constant defined by Eq. 4-15a.
δ Small increment, also defined by $\nu - 1 + \delta$.
ϵ Constant defined by Eq. 4-15c.
K Constant defined by Eq. 4-15b.
λ Elastic constant of myocardium.
μ Elastic constant of myocardium.
ν Shell elastic constant.
ρ Specific gravity of myocardium.
$\sigma_{rr}, \sigma_{\theta\theta}, \sigma_{\phi\phi}, \sigma_{cc}$ Compressive stress components, where c denotes any circumferential direction.
τ Cardiac cycle variable, 0 in diastole and 1 in full systole.

The Ellipse

Fig. 4 illustrates an ellipse with minor diameter $2a$ and major diameter $2b$ which has been rotated about its major axis. The generating ellipse has equation $(x^2/a^2) + (y^2/b^2) = 1$. Any
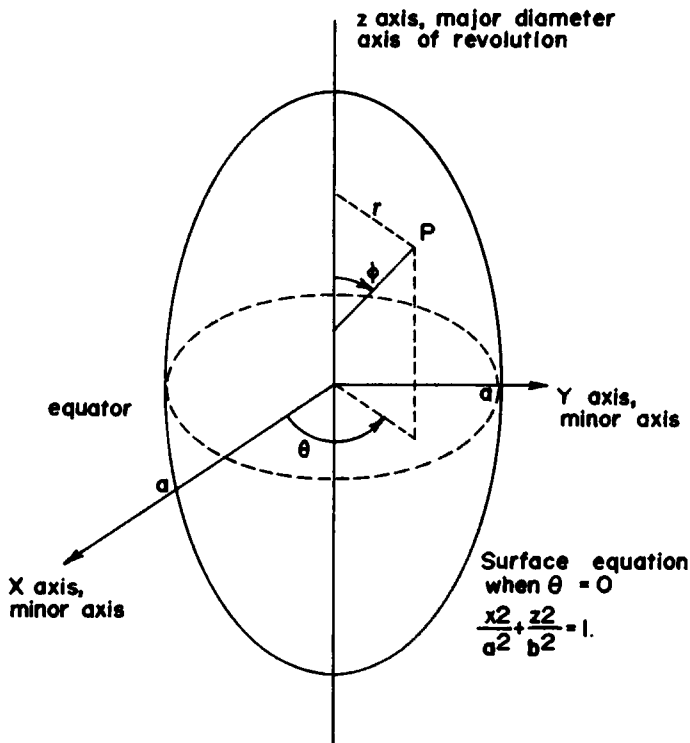

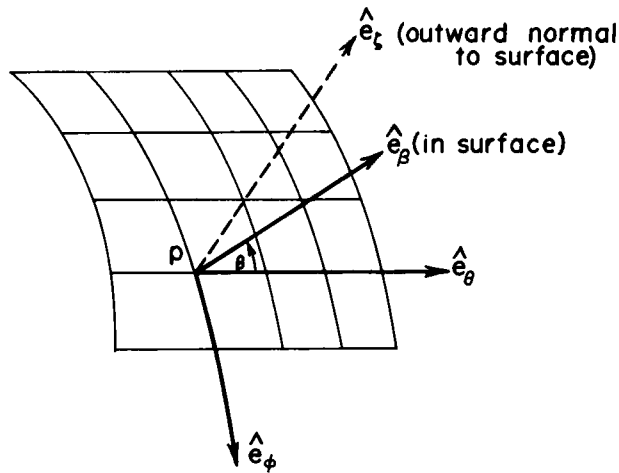FIGURE 4   Ellipsoid of revolution used as a model for an ellopsoidal thin-shelled heart.

FIGURE 5 Local unit vectors around the point P of Fig. 4.

point on the surface will have its unique values of ϕ and θ which specify the point. The distance from the general surface point to the axis of revolution is defined to be $r(\phi)$. A straightforward geometrical analysis will show that

$$r(\phi) = a \sin\left[\tan^{-1}\left(\frac{b}{a}\tan\phi\right)\right] = b \tan\phi\left[1 + \left(\frac{b}{a}\tan\phi\right)^2\right]^{-1/2} \tag{5-1}$$

Note that $r(\pi/2) = a$ and $r(0) = 0$ and that in general, $0 \leq r(\phi) \leq a$. Fig. 5 illustrates a differential region about a general ϕ, θ point on the surface. The unit vectors e_ϕ, e_β, and e_θ lie in the surface, while e_ζ is directed outward from it. The intersection of the ellipsoidal surface with the half-plane of constant θ is a curve which has radius of curvature defined to be R_ϕ. There is a plane which is perpendicular to both the constant θ plane and the surface. The intersection of this plane with the surface produces a curve which is defined to have radius of curvature R_θ. Seide (1974) shows that these are principal radii, with values

$$R_\phi = \frac{a^2}{b}\left[1 + \left(\frac{a^2}{b} - 1\right)\sin^2\phi\right]^{-3/2} \tag{5-2}$$

$$R_\theta = \frac{a^2}{b}\left[1 + \left(\frac{a^2}{b} - 1\right)\sin^2\phi\right]^{-1/2} \tag{5-3}$$

The plane normal to the surface which intersects a surface line of constant θ and angle β from e_θ will have radius of curvature which can be found using Seide's Eq. 1.1.13d. Its reciprocal is

$$\frac{1}{R_\beta} = \frac{1}{R_\phi}\sin^2\beta + \frac{1}{R_\theta}\cos^2\beta. \tag{5-4}$$

If p is a general position on the surface, then let

$$g_\phi \equiv \left| \frac{\partial p}{\partial \phi} \right| = R_\phi \qquad (5\text{-}5)$$

$$g_\theta \equiv \left| \frac{\partial p}{\partial \theta} \right| = r. \qquad (5\text{-}6)$$

These will be useful both in direct analysis here and in correlating equations with those of Seide, who uses the same definitions.

VI. TWO SPECIFIC TENSION STRAND MODELS

The Spherical, Nonintersecting, Nonterminating Model

Assume that: (a) The myocardium is a sphere. (b) All strands on a radial line run in the same direction. (c) No strands cross any other strands. (d) There is a strand which is a great circle forming angle β with the equator of the heart. (e) The number of strands per steradian is constant everywhere. (f) No strands terminate; all are closed loops.

These assumptions might initially be believed to produce a realistic model of strand geometry. The actual geometry, however, implied by these assumptions, is that of strands which resemble tilted parallels of latitude on the earth, with resulting north and south pole-like structures somewhere above and below the myocardial equator. Because the geometry of myocardial strands does not resemble tilted parallels of latitude, assumption f must be inappropriate. It therefore appears that any model of strand geometry which is compatible with the known morphology of the heart must have strands which terminate. The body forces of the myocardial fibers will therefore include both the end forces and acceleration forces discussed in section III.

The Elliptical, Iso-oblique, Terminating, Nonintersecting Model

The following model is a reasonable oversimplification of the known strand geometry of the left ventricular myocardium at a constant depth (Streeter et al., 1969). (a) The left ventricular myocardium is a thin shell whose middle surface (locus of all points equally distant from the inner and outer walls) is the ellipsoid of revolution shown in Fig. 4. (b) All strands form an acute angle β with the e_θ. (Streeter et al. [1969] observe β to vary continuously from 60° on the endocardium to $-60°$ on the epicardium.) (c) The density of strands per steradian is constant everywhere. (d) The strands terminate as necessary in order to obey assumption c. (e) All strands have the same tension at the equator $\theta = \pi$ and each has the same tension throughout its length. (f) The number of strands is so large that continuum equations can be applied. (g) The tension for an area dA on a surface normal to the middle surface and at an angle $\beta + \pi/2$ to the $\hat{e}_\theta$ vector is $F_a\, dA$. Integrated over the $\hat{e}_\zeta$ direction, this force will be $F_L\, dl$, where dl is the element of length in the direction with angle $\beta + \pi/2$ from e_θ. A map of the strand model is shown in Fig. 6, assuming the major-to-minor axis ratio of the heart is b/a.

Let $\overline{N}_{\phi_0}$ strands cross the surface perpendicular to the middle surface which intersects it at the curve $\phi = \phi_0$. $\overline{N}_{\pi/2}$ is the number of strands crossing the equator. Let $\hat{e}_\beta = \hat{e}_\phi \cos \beta - \hat{e}_\phi \sin$
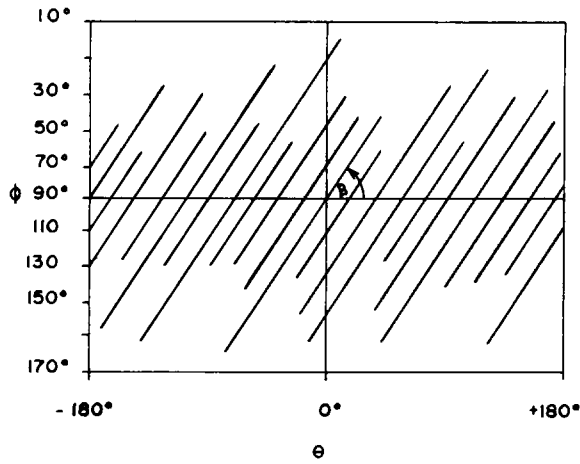
FIGURE 6 A θ, ϕ diagram, resembling a Mercator map, for the strands of myocardial fibers in the ellipsoidal, iso-oblique, terminating, nonintersecting model of the heart. The diagonal lines represent myocardial fibers. They terminate at different "latitudes" in the iso-oblique model.

β. Let R_ϕ be the radius of curvature of the middle surface in the plane of constant θ, and let R_θ be the radius of curvature in the plane of constant ϕ. Assumption c requires that

$$\frac{\overline{N_\phi}}{N_{\pi/2}} = \frac{r(\phi)}{r(\pi/2)} = \frac{r(\phi)}{a}. \tag{6-1}$$

If the strands were projected into the middle surface, each would occupy an interval along the equator of $2\pi/N_{\pi/2}$ rads at the equator in the $\hat{e}_\theta$ direction. Off the equator, each would occupy the same distance in the $\hat{e}_\theta$ direction by assumption d. The tension of an individual strand, by assumption g, would be

$$F_L 2\pi a(\sin \beta)/N_{\pi/2}. \tag{6-2}$$

The terminal body force per area acting upon the middle surface can be evaluated using Eqs. 3-4, 6-11, 6-2, and 5-7:

$$F_{\text{term}} = \frac{\hat{e}_\beta F_L \sin \beta}{r(\phi)R_\phi} \frac{\partial r(\phi)}{\partial \phi}. \tag{6-3}$$

If the ellipsoid were a perfect sphere, the above equation would simplify to $F_L R_\theta^{-1} \sin \beta \cot \phi$. It appears that the above force density becomes infinite at the poles, where its net effect is an expansion of the pole area, plus (provided $\beta \neq \pi/2$) a torque.

The acceleration body force per surface area can be evaluated using Eqs. 3-9, 5-6, and 5-7. It is

$$F_{\text{acc}} = -\hat{e}_\zeta \frac{F_L}{R_\beta} = -\hat{e}_\zeta F_L \left[\frac{1}{R_\phi} \sin^2 \beta + \frac{1}{R_\theta} \cos^2 \beta \right]. \tag{6-4}$$

Note that the force normal to the middle surface in the iso-oblique model is only the above acceleration force, and that it becomes constant when the ellopsoid becomes a sphere, while the terminating body force retains its variation in ϕ.

VII. THE ELLIPSOIDAL, THIN-SHELLED MODEL WITH AXIALLY SYMMETRIC BODY FORCES

The purpose of this section is to analyze a heart with systolic body forces under the following assumptions: (*a*) The heart is a thin shell of constant thickness *h*. (*b*) The middle surface of the heart is defined as the locus of all points of equal distance from the endocardial and epicardial surfaces. The middle surface is assumed to be an ellipsoid of revolution of minor diameters 2*a* in the lateral and dorsal-ventral direction, and a major diameter of 2*b* in the cephalocaudal direction. Fig. 4 shows the ellipsoid for an upright human. (*c*) The elastic properties of the heart are linear and transversely isotropic, which means all displacements are small enough for a first-order elastic theory to be valid. (*d*) The body forces on the heart have bounded force per area, have no circumferential components, and are independent of circumferential position. (*e*) The membrane shell specifications are applicable. This is equivalent to assuming that the elastic energy stored in the bending of the heart bent about either axis in the middle surface is negligible compared with elastic energy stored in tension and shearing forces whose moments are normal to the middle plane. (*f*) The analysis will be a static equalibrium one in which inertial forces are neglected.

These assumptions reduce the general three-dimensional heart into two dimensions by means of the thin-shell approximation. The lack of circumferential variability of body forces, and lack of circumferential components of body forces, reduce the problem to one dimension. The membrane assumption, which is physically quite reasonable, eliminates the need to solve a difficult fourth-order differential equation whose solutions are not known explicitly.

The General Solution to the Ellipsoidal Model

The solution to the problem as formulated is available from the theory of shells. The exposition here will be based upon the notation and equations of Seide (1975), except as noted.

The geometry assumed is shown in Figs. 2 and 3. A point which has surface coordinates $\phi = \phi_0$, $\theta = \theta_0$, $\zeta = 0$ before application of body and boundary forces will have coordinates $\phi = \phi_0 + u_\phi$, $\theta = \theta_0$, $\zeta = u_\zeta$ after application of boundary and body forces. (Siede (1975) uses w where I use u_ζ). Note that u_ϕ and u_ζ are functions of ϕ only.

The strains are defined by the following functions of displacement vector u:

$$\epsilon_\bullet = \frac{1}{R_\phi}\left(\frac{du_\phi}{d\phi} + u_\zeta\right) \tag{7-1}$$

$$\epsilon_0 = \frac{1}{R_\theta}(u_\zeta + u_\phi \cot \phi). \tag{7-2}$$

The stresses on the elastic skeleton of the heart will be given by

$$N_\phi = \int_{-h/2}^{h/2} \sigma_\phi\left(1 + \frac{\zeta}{R_\phi}\right)d\zeta = K(\epsilon_\phi + \nu\epsilon_\theta) \tag{7-3}$$

$$N_\theta = \int_{-h/2}^{h/2} \sigma_\theta\left(1 + \frac{\zeta}{R_\phi}\right)d\zeta = K(\epsilon_\theta + \nu\epsilon_\phi), \tag{7-4}$$

where h is the shell thickness and K and ν are elastic constants.

The effects of both true body forces from contractile elements (as formulated in section III) and hydrostatic pressure on the endocardial and epicardial surfaces will be accounted for by using a force density per area which is applied to the middle surface. The surface element described by $\phi_0 \leq \phi \leq \phi_0 + d\phi$, $\theta_0 \leq \theta \leq \theta_0 + d\theta$ will have area $dA = g_\phi g_\sigma d\phi d\theta$ and force vector whose (ϕ, θ, ζ) components are $(q_\phi dA, 0, q_\zeta dA)$.

The relationship between the stresses and strains, under the equilibrium and other assumptions of this section, will be given by

$$\frac{1}{R_\phi} \frac{d}{d\phi} (N_\phi R_\theta \sin \phi) - N_\theta \cos \phi + R_\theta q_\phi \sin \phi = 0 \qquad (7\text{-}5)$$

$$\frac{N_\phi}{R_\phi} + \frac{N_\theta}{R_\theta} - q_\zeta = 0. \qquad (7\text{-}6)$$

Eq. 7-6 is Laplace's law as applied to thin shells. Note that it alone does not give the solution, since Eq. 7-5 must also be used for force equilibrium, even when q_ϕ is zero. Furthermore q_ϕ is not zero when the strands terminate, and as inferred in section VI, actual strands apparently terminate.

If the membrane assumptions were not made, it would first be necessary to use equations in Seide (1975), such as Eqs. 7.1.2f, 7.1.6a, and 7.1.11a to define and solve for intermediate variables Θ and U. In the membrane approximation, however, Θ and U are identically zero. Consequently, the general solution simplifies to the following special case of Seide's Eq. 7.1.13a, which has been rearranged somewhat and given the membrane and geometric assumptions used here.

$$\frac{d}{d\phi}\left(\frac{U_\phi}{\sin \phi}\right) = \frac{R_\phi R_\theta g_\zeta(\phi)}{Eh} \left\{ \frac{\nu(2I - 1)}{\sin \phi} + \left[\frac{(R_\phi^2 + R_\theta^2)I - R_\theta^2}{R_\phi R_\theta \sin \phi}\right]\right\} \qquad (7\text{-}7)$$

$$u_\zeta = \frac{1}{Eh}\left[q_\zeta R_\theta^2 - \left(\frac{R_\theta}{R_\phi} + \nu\right)I\right] - u_\phi \cot \phi \qquad (7\text{-}8)$$

where

$$I = \int_0^\phi H(\phi, \hat{\phi}) \frac{\hat{\phi}}{\phi^2} d\hat{\phi} \qquad (7\text{-}9)$$

$$H(\phi, \hat{\phi}) = \left[\frac{q_\zeta(\hat{\phi})}{q_\zeta(\phi)} \cos \hat{\phi} - \frac{q_\phi(\hat{\phi})}{q_\zeta(\phi)} \sin \hat{\phi}\right] \left[\frac{R_\phi(\hat{\phi}) R_0(\hat{\phi})(\sin \hat{\phi}) \phi^2}{R_\phi(\phi) R_0(\phi) \hat{\phi} \sin^2 \phi}\right]. \qquad (7\text{-}10)$$

Eqs. 7-7 and 7-8 appear to be singular where $\sin \phi = 0$. However, $H(0, 0) = 1$, so that for small ϕ and $\hat{\phi}$ a Taylor series expansion of $H(\phi', \hat{\phi})$ about $(0, 0)$ yields

$$I \simeq \frac{1}{2} + \frac{\phi}{3} \frac{\partial H}{\partial \hat{\phi}}\bigg|_{0,0} + \frac{\phi}{2} \frac{\partial H}{\partial \phi}\bigg|_{0,0}. \qquad (7\text{-}11)$$

This equation implies that $(2I - 1)/\sin \phi$ is finite at $\phi = 0$. As ϕ approaches zero, R_ϕ approaches R_θ, and use of the equations for R_ϕ, R_θ, and Eq. 7-11 shows that the bracketed term in Eq. 7-7 approaches

$$\left[\frac{R_\phi^2 + R_\theta^2}{3R_\phi R_\theta}\right]\left[\frac{\partial H}{\partial \phi}\bigg|_{0,0} + \frac{3}{2}\frac{\partial H}{\partial \phi}\bigg|_{0,0}\right] \qquad (7\text{-}12)$$

so that Eq. 7-7 is not singular. The thin-shell theory has provided Eqs. 7-7 and 7-8, which then have to be integrated by numerical methods.

The change in volume produced by the given body force is approximately

$$\Delta V = \int_0^\pi \int_0^{2\pi} u_\zeta g_\theta g_\phi \,d\theta d\phi = \int_0^\pi \int_0^{2\pi} u_\zeta R_\phi r \,d\theta d\phi. \qquad (7\text{-}13)$$

VIII. CONCLUSIONS

There are now three known ways of accounting for systolic forces in a three-dimensional model of the heart: (*a*) Tension in one circumferential direction may be assumed to be zero, negative tensions may be assumed not to exist, and effects of end forces may be neglected, thereby permitting Laplace's law to be used to solve for the tensions (Streeter et al., 1969). (*b*) The tension strand model of this paper can be invoked and the body forces from strand termination and strand acceleration may be used as forcing terms in the elastic differential equations. (*c*) A dilation term may be placed in the elastic strain solution so as to represent the effects of the stress forces actively generated. (Ghista, 1974).

The second of these approaches has the advantage of total rigor, conceptual clarity, and explicit evaluation of both terminal and acceleration forces. It has the disadvantage of increased analytical difficulty.

The analysis of section IV, which was the first to show that all three of the compressive tensor stresses can be supraluminal, is definite theoretical evidence favoring the hypothesis that left ventricular capillary pressure can exceed luminal pressure. When this is combined with the experimental evidence reviewed in section II, I believe that it is reasonable to conclude that coronary capillary pressure sometimes exceeds luminal pressure.

Direct visual observation of severed coronary veins (Woods, 1892) and phasic tracings of flow in coronary veins (Gregg, 1950) suggest that practically all of the coronary venous outflow occurs in systole. Later evidence (Berne and Rubio, 1979, p. 900) includes somewhat different tracings, which some authorities interpret as indicating that coronary sinus flow is augmented (in both systole and diastole) by reduced pleural cavity pressure in the respiratory cycle. The exact reasons for phasic fluctuations in coronary venous outflow are unknown, although Wiggers (1954) has suggested that the blood is "massaged out" of the heart in systole. I suggest that supraluminal intramyocardial pressure may be involved in this "massaging" action, since the supraluminal pressure, like the fastest venous outflow, occurs in systole.

Kirk and Honig's requirement that supraluminal pressure cannot occur without tissue compression is straightforward after systolic ejection has begun. During isovolumic contraction it was extended to include compression secondary to net ejection of blood from the myocardial vascular system. In effect, middle-wall pressures can exceed luminal pressures if the endocardium has contracted so that it is under compression. Since myocardial infarctions usually proceed from endocardium outwards, the relevance of the inferred endocardial compression should be kept in mind as one possible factor which may make the endocardium more vulnerable to infarction.

Having placed systolic supraluminal intramyocardial capillary pressure upon a more solid theoretical foundation, we can now use it as a working hypothesis in the design of further experiments and theoretical models.

REFERENCES

ARCHIE, J. P., JR. 1975. Intramyocardial pressure effect of preload on transmural distribution of systolic coronary blood flow. *Am. J. Cardiol.* **35**:904–911.

ARMOUR, J. A., and W. C. RANDALL. 1971. Canine left ventricular pressures. *Am. J. Physiol.* **220**:1833–1839.

BAIRD, R. J., R. T. MANKTELOW, P. A. SHAH, and F. M. AMELI. 1970. Intramyocardial pressure: a study of its regional variations and its relationship to intraventricular pressure. *J. Thorac. Cardiovasc. Surg.* **59**:810–823.

BERNE, R. M., and R. RUBIO. 1979. Coronary Circulation. *In* Handbook of Physiology, sect. 2, The Cardiovascular System, vol. 1, The Heart. R. M. Berne, N. Sperelakis, and S. R. Geiger, editors. The Williams & Wilkins Company, Baltimore. 873–952.

BRANDI, G., and M. McGREGOR. 1969. Intramural pressure on the left ventricle of the dog. *Cardiovasc. Res.* **3**:472–275.

BRAUNWALD, E., J. ROSS, Jr., and E. H. SONNENBLICK. 1976. Mechanisms of contraction of the normal and failing heart. 2nd ed. Little, Brown & Co., Boston.

BURTON, A. C. 1957. The importance of the shape and size of the heart. *Am. Heart J.* **54**:801–10.

DIEUDONNE, J. M. 1967a. Tissue-cavitary difference pressure of dog left ventricle. *Am. J. Physiol.* **213**:101–106.

DIEUDONNE, J. M. 1967b. Tissue-cavitary difference pressure of dog myocardium under stress. *Am. J. Physiol.* **213**:107–111.

D'SILVA, J. L., D. MENDEL, and M. C. WINTERTON. 1963. Effect of symptomatic amines on intramyocardial pressure in the rabbit. *Am. J. Physiol.* **205**:10–16.

GHISTA, D. N. 1974. Rheological modeling of the intact left ventricle. *In* Cardiac Mechanics: Physiological, Clinical, and Mathematical Considerations. J. M. Mirsky, D. N. Ghista, and H. Sandler, editors. John Wiley & Sons, Inc., New York.

GHISTA, D. N., and H. SANDLER. 1969. Analytic elastic-viscoelastic model for the shape and the forces in the left ventricle. *J. Biomech.* **2**:35–47.

GOOD, E. S., R. E. MATES, and H. FALSETTI. 1974. A model of cardiac muscle dynamics. *Circ. Res.* **35**:184–196.

GOULD, P., D. N. GHISTA, L. BROMOBOLICH, and I. MIRSKY. 1972. *In vivo* stresses in the human left ventricular wall: analysis accounting for the irregular three-dimensional geometry and comparison with idealized geometry analyses. *J. Biomech.* **5**:521–539.

GREGG, D. L. 1950. Coronary Circulation in Health and Disease. Lea & Febiger, Philadelphia.

GREGG, D. E., and R. W. EKSTEIN. 1941. Measurements of intramyocardial pressure. *Am. J. Physiol.* **132**:781–790.

HOOD, W. P., W. J. THOMLSON, C. E. RACKLES, and E. L. ROLETT. 1969. Comparison of calculation of left ventricular wall stress in man from thin-walled and thick-walled ellipsoidal models. *Circ. Res.* **24**:575–582.

JOHNSON, D. R. and J. R. DiPALMA. 1939. Intramyocardial pressure and its relation to aortic blood pressure. *Am. J. Physiol.* **125**:234–243.

KANE, R. L., T. A. McMAHON, R. L. WAGNER, and W. H. ABELMAN. 1976. Ventricular elastic modulus as a function of age in the Syrial golden hamster. *Circ. Res.* **38**:74–80.

KIRK, E. S., and C. R. HONIG. 1964. An experimental and theoretical analysis of myocardial tissue pressure. *Am. J. Physiol.* **207**:361–167.

LOVE, A. E. H. 1927. A Treatise on the Mathematical Theory of Elasticity, 4th ed. Reprinted in 1944 by Dover Publications, Inc., New York.

MIRSKY, I. 1969. Left ventricular stresses in the intact human heart. *Biophys. J.* **9**:189–208.

MIRSKY, I. 1973. Ventricular and arterial wall stress based on large deformation analyses. *Biophys. J.* **13**:1141–1159.

MIRSKY, I. D. 1974. Review of various theories for the evaluation of left ventricular wall stresses. *In* Cardiac Mechanics: Physiological, Clinical, and Mathematical Considerations. I. D. Mirsky, D. N. Ghista, and H. Sandler, editors. John Wiley & Sons, Inc., New York. 381–409.

MIRSKY, I., and W. W. PARMLEY. 1973. Assessment of passive elastic stiffness for isolated heart muscle in the intact heart. *Circ. Res.* **33**:233–243.

PAO, Y. C., E. L. RITMAN, and E. H. WOODS. 1974. Finite-element analysis of left ventricular myocardial stresses. *J. Biomech.* **7**:469–477.

PIFARRE, R. 1968. Intramyocardial pressure during systole and diastole. *Ann. Surg.* **168**:871–875.

RANKIN, J. S., C. E. ARENTZEN, P. A. McHALE, D. LING, and R. W. ANDERSEN. 1977. Viscoelastic properties of the diastolic left ventricle in the conscious dog. *Circ. Res.* **41**:37–45.

SALISBURY, P. F., C. E. CROSS, and P. A. RIEBEN. 1962. Intramyocardial pressure and strength of left ventricular contraction. *Circ. Res.* **10**:608–623.

SANDLER, H., and H. T. DODGE. 1963. Left ventricular tension and stress in man. *Circ. Res.* **13**:91–104.

SEIDE, P. 1975. Small Elastic Deformations of Thin Shells. Sijthoff & Noordhoff International Publishers, The Netherlands.

STREETER, D. D., Jr., S. M. SPOTNITZ, D. P. PATEL, J. ROSS, Jr., and E. H. SONNENBLICK. 1969. Fiber orientation in the canine left ventricle during diastole and systole. *Circ. Res.* **24**:339–347.

STREETER, D. D., Jr., R. N. VAISHNAV, D. J. PATEL, H. M. SPOTNITZ, J. ROSS, Jr., and E. H. SONNENBLICK. 1970. Stress distribution in the canine left ventricle during diastole and systole. *Biophys. J.* **10**:345–363.

TILLMANNS, H., S. IKEDA, H. HANSEN, J. S. M. SARNIA, J. M. FAUVEL, and R. J. BING. 1974. Microcirculation in the ventricle of the dog and turtle. *Circ. Res.* **34**:561–569.

VAN DER MEER, J. J., R. S. RENEMAN, H. SCHNEIDER, and J. WIEBERDINK. 1970. A technique for estimating intramyocardial pressure in acute and chronic experiments. *Pflug. Arch. Eur. J. Physiol.* **314**:162.

WIGGERS, C. J. 1954. The interplay of coronary vascular resistance and myocardial compression in regulating coronary flow. *Circ. Res.* **2**:271–279.

WOODS, R. N. 1892. A few applications of a physical theorem to membranes in the human body in a state of tension. *J. Anat. Physiol.* **26**:360–370.

WONG, A. Y. K., and P. M. RAUTAHARJU. 1968. Stress distribution within the left ventricular wall approximated as a thick ellipsoidal shell. *Am. Heart J.* **75**:649–662.